ARTICLE IN PRESS
JID: AOSL [m5GeSdc;March 4, 2026;0:42]
Atmospheric and Oceanic Science Letters xxx (xxxx) xxx
Contents lists available at ScienceDirect
Atmospheric and Oceanic Science Letters
journal homepage: http://www.keaipublishing.com/en/journals/atmospheric-and-oceanic-science-letters/

Planetary boundary layer heights over a sharp vegetation-contrast area during the DECODE field campaign

Lanqiang Bai[a], Zhiyong Meng[b,*], Quxin Cui[b], Chenggang Wang[c]

[a] Foshan Tornado Research Center, and China Meteorological Administration Tornado Key Laboratory, Guangdong, China
[b] Department of Atmospheric and Oceanic Sciences, School of Physics, Peking University, and China Meteorological Administration Tornado Key Laboratory, Beijing, China
[c] School of Atmospheric Physics, Nanjing University of Information Science and Technology, Nanjing, China

A R T I C L E I N F O

Keywords:
Boundary layer height
Radiosonde
Sharp vegetation contrast
DECODE

关键词:
大气边界层高度
探空
植被覆盖差异
DECODE

A B S T R A C T

During the DEsert–Oasis COnvergence line and Deep convection Experiment (DECODE) field campaign, conducted from 5 July to 9 August 2022, an unprecedented number of daytime balloon-borne soundings were collected over the Hetao region in North China. Using these high-resolution observations, this study investigates the observational characteristics of planetary boundary layer heights (PBLHs) over this sharp vegetation-contrast area, where daytime PBLH measurements have been rarely available. A total of 386 soundings ranging from 1100 to 1800 LST were selected to derive PBLHs at multiple sites across irrigated croplands and deserts. During this period, the PBLHs across all sites average around 2000 m above ground, with a diurnal peak reaching approximately 2500 m. These sites occasionally experience exceptionally deep PBLs, reaching up to about 6000 m above mean sea level, when the lower troposphere exhibits weak stability associated with an upper-level cold low. The PBLHs over irrigated croplands are generally lower than those over desert areas, although the difference shows considerable variability, ranging from several hundred to more than a thousand meters.

摘要

在2022年7–8月开展的 “沙漠–绿洲辐合线与深对流观测试验(DECODE)” 中, 试验团队在华北河套地区白天密集开展了数百次小球探空观测. 基于这些稀有的高时空分辨率资料, 系统分析了沙漠与灌溉农田等植被反差显著区域的大气边界层高度(PBLH)特征. 结果显示, 白天边界层平均高度约为2000米, 午后可发展至约2500米; 在高空冷涡影响, 低层大气稳定度较弱的条件下, 边界层有时可显著加深, 最高接近海拔6000米. 总体而言, 灌溉农田上空的边界层高度低于沙漠区域, 但两者差异具有明显的变率, 幅度从数百米到上千米不等.

1. Introduction

The Yellow River (Fig. 1(a)) has been vital for agriculture throughout Chinese history, supporting civilizations with irrigation and fertile soil. It also serves as a transportation route and a source of freshwater. Irrigated by the Yellow River, an oasis area known as the Hetao irrigation district has developed in the western part of Inner Mongolia, creating a sharp vegetation contrast (Fig. 1(b)). Surrounding this irrigation oasis is arid and semi-arid land, including the Kubuqi Desert to the south. This land use contrast often produces thermally induced local circulations near the oasis–desert border, like sea-breeze circulations along coastlines (Huang et al., 2019). The near-ground convergent zone associated with the oasis–desert contrast is frequently observed to contribute the cloud formation and afternoon thunderstorms in this region (Huang et al., 2019; Kawase et al., 2008; Liu et al., 2023; Sato et al., 2007), which motivated the DEsert-oasis COnvergence line and Deep convection Experiment (DECODE) field campaign in the summer of 2022 (Meng et al., 2024).

This sharp vegetation-contrast area produces a prominent surface heat flux heterogeneity in the daytime, especially in summer afternoons. Near-surface mixing is encouraged on the desert sides (desert amplification) while suppressed on the oasis sides, leading to the difference in the growth of the planetary boundary layer (PBL). As the lowest part of the atmosphere, PBL processes are crucial for local severe weather. The PBL height (PBLH) is a crucial variable for characterizing the PBL state, as it determines the height for the exchange of momentum, moisture, and chemical compounds between the surface and the free troposphere (Garratt, 1994; Hu et al., 2010; Stull, 1988; Seibert et al., 2000; Seidel et al., 2010). Various instruments, including radiosondes, sodars, ceilometers, backscatter lidars, and Doppler wind lidars, have

Peer review under the responsibility of Editorial Board of Atmospheric and Oceanic Science Letters.
* Corresponding author.
E-mail address: zymeng@pku.edu.cn (Z. Meng).

https://doi.org/10.1016/j.aosl.2026.100782
Received 7 November 2025; Revised 17 December 2025; Accepted 12 January 2026
Available online xxx

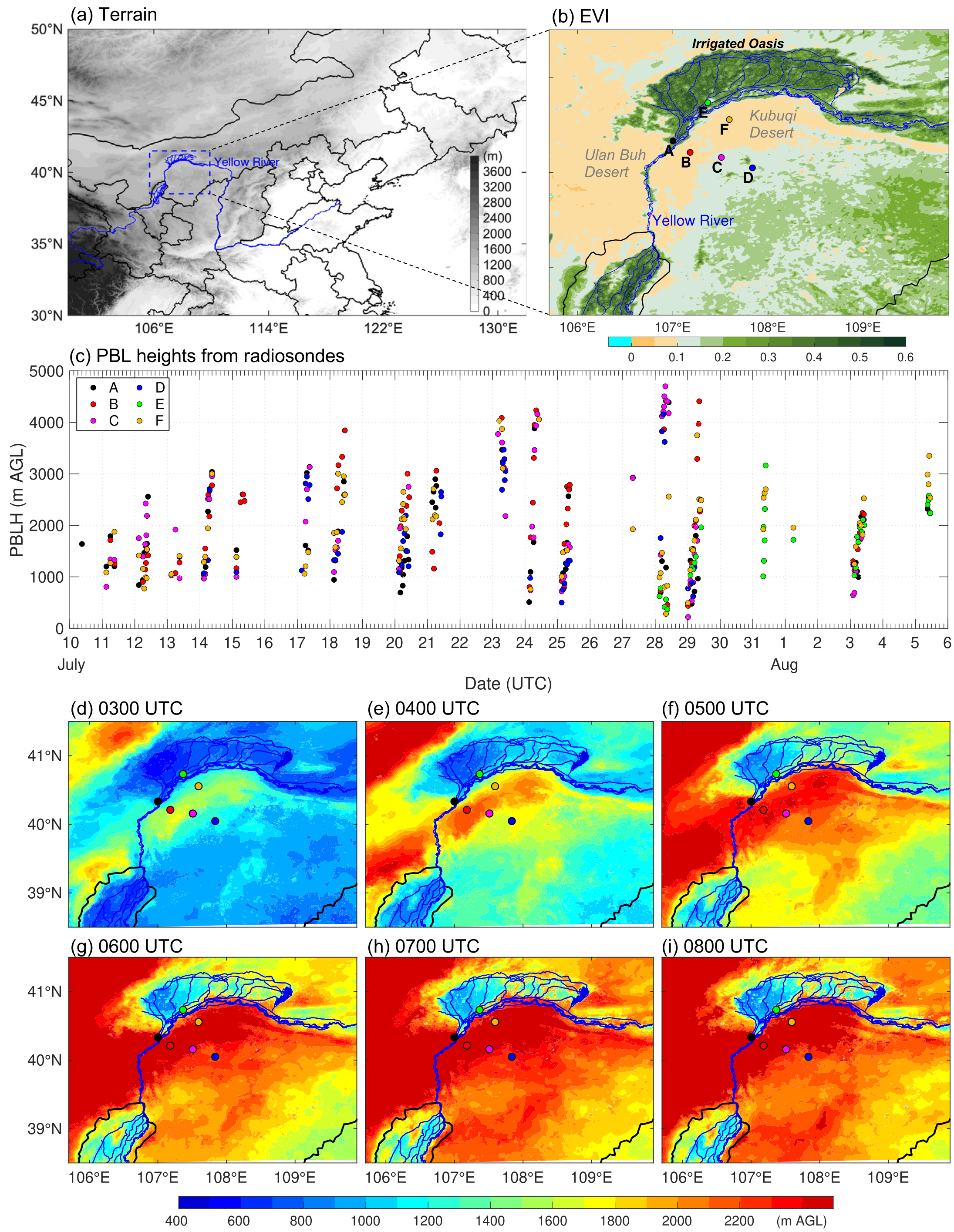

Fig. 1. (a) Terrain heights (units: m) with the Yellow River shown in blue. (b) Enhanced Vegetation Index (EVI; average during June–August from 2012 to 2016) zoomed in within the rectangle in (a). The IOP sites are marked by the dots labeled A, B, C, D, E, and F. (c) PBLHs at the six IOP sites obtained from the 386 radiosondes. The numbers on the *x*-axis represent 0000 UTC for each day. (d–i) Spatial distributions of the WRF-based (1-km grid spacing) PBLHs averaged over the period from 10 July to 5 August 2022.

been utilized for detecting PBLH, each having its own strengths and limitations (Beyrich, 1997; Chan and Wood, 2013; Dai et al., 2014; Eresmaa et al., 2006; Hennemuth and Lammert, 2006; Sawyer and Li, 2013; Seibert et al., 2000, 2010; Zhou, 2021).

Climatological studies of PBLH estimated from radiosonde data (Guo et al., 2016) and Global Navigation Satellite System radio occultation data (Kalmus et al., 2022) indicate that the Hetao irrigation district features a PBLH of approximately 2 km above ground level (AGL) during the afternoon of the convectively active season (June, July, and August). In this area, only one conventional radiosonde is operationally launched twice a day, at 0800 and 2000 LST (local standard time), respectively (LST = UTC + 8 h). The observed characteristics of the PBL in the afternoon when convection is active are thus limited. On the other hand, there being only one operational radiosonde makes it impossible to characterize the horizontal heterogeneity of the PBLH across the oasis and desert land use.

During the intensive observation periods (IOPs) of the DECODE field campaign from 5 July to 9 August 2022, hundreds of radiosondes were launched throughout the day at six sites, as illustrated in Fig. 1(b). These fine-resolution radiosonde observations provide a tremendous opportunity to depict the diurnal cycle of the PBLH and the differences in PBLH associated with varying land use in this region. The objective of this study is to reveal the daytime PBLHs at the six sites over the oasis–desert area using the intensive radiosonde observations during the DECODE field campaign.

2. Data and methods

Fig. 1(b) illustrates the geographic locations of the balloon radiosondes launched during the IOPs of the DECODE field campaign. The radiosondes utilize a 50-cm helium-filled balloon, and the observation errors below 5 km AGL are less than 0.3 K for temperature, 0.5 hPa for pressure, 4% for relative humidity, 0.5 m s^{-1} for wind speed, and 5° for wind direction (Han et al., 2017). From 8 July to 5 August 2022, data from a total of 695 valid radiosondes were collected with 154, 123, 138, 93, 33, and 154 sounding profiles at sites A, B, C, D, E, and F, respectively (Fig. 1(b)). The vertical resolution of the available sounding data is nearly every 1 s per balloon rising. Basic quality control procedures were conducted to remove bad sounding profiles by a manual inspection of skew *T*–log *p* diagrams. To remove the raw data noises, the 9-point running average was performed for all variables of these vertical profiles. To get a sense of the daytime PBLH in the arid/semiarid areas, only the valid soundings from 0300 to 1000 UTC were selected because it is relatively easy to estimate the heights of well-mixed PBLs.

Prior studies have suggested that the calculated PBLH can yield non-negligible variabilities using different estimation methods (Seidel et al., 2010). The bulk Richardson number (*Ri*) method (Vogelezang and Holtslag, 1996) is demonstrated to be a robust method for both the stable layer and convective boundary layer (CBL) and thus suitable to conduct PBLH climatology analysis such as that in Europe, the United States, and Asia (Guo et al., 2016; Seidel et al., 2012):

$$Ri(z) = \frac{(g/\theta_{vs})(\theta_{vz} - \theta_{vs})(z - z_s)}{(u_z - u_s)^2 + (v_z - v_s)^2}, \tag{1}$$

where g is the acceleration due to gravity, z is height, s denotes the surface level, θ_v is virtual potential temperature, u and v are the zonal and meridional wind speed. Here, the surface friction velocity is ignored due to its small magnitude compared with other terms. The bulk *Ri* represents the ratio of turbulence associated with buoyancy to that induced by mechanical shear. The PBLH is typically determined as the lowest level at which the bulk *Ri* is lower than a critical value (e.g., 0.25) when the laminar flow becomes unstable (Seidel et al., 2012).

In this study, we first estimated the PBLH using the bulk *Ri* method and threshold described in Guo et al. (2016), which produced reasonable results for most sounding profiles (e.g., Fig. 2(a)). We then applied a manual, multi-parameter check to ensure reliable PBLH determination, particularly for cases in which relative humidity or wind shear exerted a dominant influence on the PBLH calculation. For instance, in the afternoon on 28 July 2022 when the irrigated area is cloud free, a salient capping inversion exhibits above 416 m AGL at 0700 UTC based on the temperature profile at site E (Fig. 2(c)). Below this capping inversion, the nearly neutral temperature profile indicates a well-defined CBL and thus the analyzed PBLH is 416 m. Using the bulk *Ri* method, the PBLH is estimated at 958 m AGL, primarily due to the significant drying with height below this layer. This phenomenon results from the moistened air on the irrigated sides compared to the surrounding desert areas. It suggests that the relative humidity is a significant factor contributing to the uncertainty in PBLH estimation on the oasis sides. The use of the manual, multi-parameter method is a methodological choice tailored to the heterogeneous land use of the oasis–desert region.

Considering that the daytime PBLs in summer tend to be well mixed due to the strong sensible heat flux and thus the resultant buoyancy is the dominant mechanism that drives the turbulence in the CBL, the PBLH in the present study is primarily determined based on the potential temperature profiles. The level at which potential temperature increased abruptly by 1 K within a 250-m layer was first identified, and the sounding profile was then manually evaluated given the limited number of cases. If an inflection point (sharp rather than smooth changes) was well defined, the PBLH was determined at that level. When the inflection point was unobvious (e.g., Fig. 2(b)), a specific height in this layer was determined as the PBLH when this level was characterized by an evident discontinuity in relative humidity, wind speed, or wind direction (e.g., Fig. 2(e–i)). In situations where the inflection points for all variables were hard to distinguish, the evolution of sounding profiles at the preceding and subsequent adjacent times was used for an integrated assessment.

To avoid the contamination of cold pools, the sounding data influenced by precipitation were eliminated. Additionally, if determining a PBLH is debatable, the corresponding sounding data were eliminated in this study. Finally, a total of 386 valid soundings were obtained during the period of 0300–1000 UTC.

3. Results and discussion

3.1. General characteristics of PBLHs in the arid/semiarid areas

The statistics of the 386 valid soundings suggest that the oasis sites E and A are characterized by generally lower PBLH than the desert sites (Fig. 1(c)). The desert sites B and C generally feature the highest PBLHs. At site C, some unusual high-range PBLHs can reach nearly 4700 m AGL (refer to the magenta dots on 28 July in Fig. 1(c)). During 0300–1100 UTC, the average PBLH for the six sites is 1953 m AGL. The average PBLH increases from 1176 m AGL at 0300 UTC to a diurnal peak of 2537 m AGL at 0700 UTC (Fig. 3). At the peak time of 0700 UTC, the average PBLHs for sites A–F are 2420, 2718, 2904, 2503, 1250, and 1639 m AGL, respectively. It is worth noting that sites E and F individually have only three samples at 0700 UTC.

Sites E and F represent a pair of typical oasis and desert locations. During the daytime, a lower PBLH at site E is expected because of the oasis–desert thermal contrast. Fig. 3 shows that the PBLHs at site E are generally lower than those at site F; however, the height difference exhibits significant uncertainty. On 3 August 2022, the two sites exhibit a minimal difference, with the mean PBLH at site E being 170 m lower than that at site F. On 31 July and 5 August, the mean PBLH differences between sites F and E are 1180 and 538 m, respectively. When a convergent boundary associated with the oasis–desert thermal contrast exists between sites E and F (28, 29, and 31 July; 1, 3, and 5 August), the average PBLH during 0600–0900 UTC over these days is 1905 m AGL at site E and 2348 m AGL at site F.

In addition to the fine-resolution sounding observations, real-time WRF-ARW forecasts during the DECODE field campaign were used to provide an overview of PBLH characteristics across the broader target region. The innermost domain employed a 1-km grid spacing to better resolve the land-use heterogeneity of the Hetao area. The Pleim–Xiu land surface model (Xiu and Pleim, 2001) was applied. Further details on the WRF forecasts are provided in Meng et al. (2024). The WRF-based PBLHs were calculated using the bulk *Ri* method with a critical value of 0.25. The western portion of the irrigated area exhibits distinctly lower PBLHs compared with the surrounding arid surfaces (Fig. 1(d–i)). Consistent with the radiosonde-derived diurnal cycle, the simulated PBLH peaks around 0700–0800 UTC. Desert sites B and C produce the highest simulated PBLHs. The oasis site E shows lower PBLHs than the nearby desert site F. Although the model reproduces the overall spatial patterns reasonably well, it tends to overestimate surface temperature and sensible heat flux when compared with other DECODE surface measurements (Meng et al., 2024). Differences among land surface model configurations also contribute to variability in the magnitude and spatial distribution of the simulated PBLH.

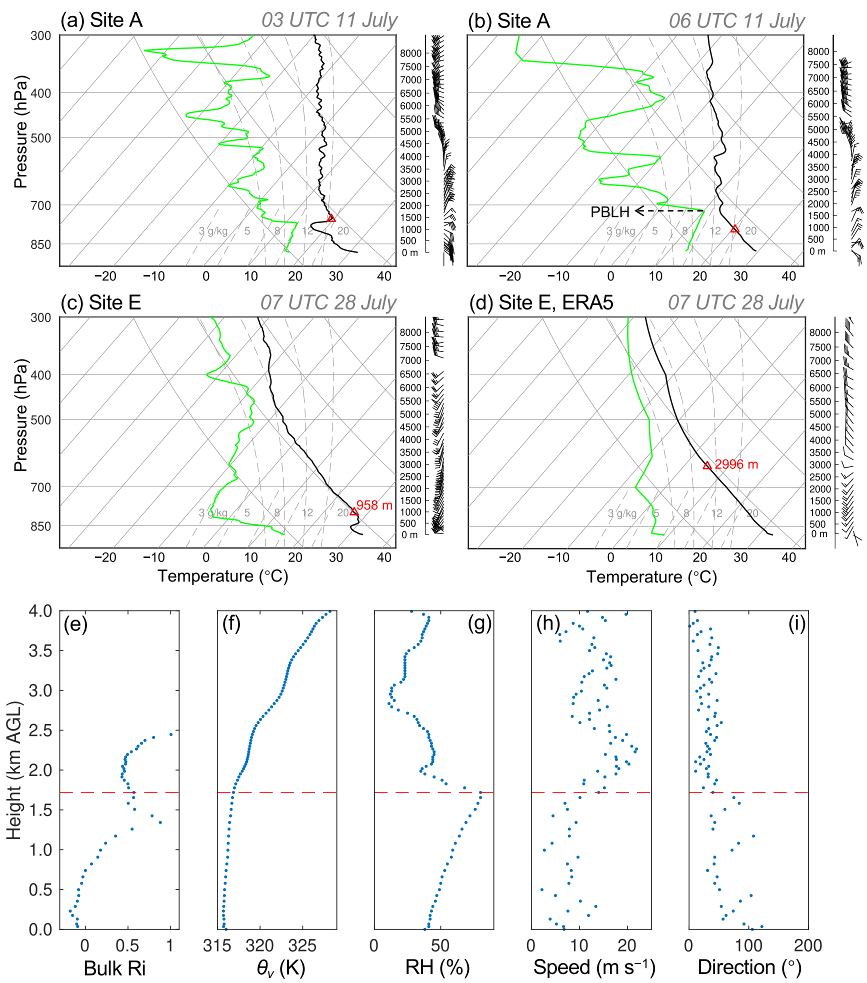

Fig. 2. Skew *T*–log *p* diagrams for the radiosonde observations at (a) 0300 and (b) 0600 UTC 11 July at site A, and at 0700 UTC 28 July at site E. The corresponding ERA5 sounding profile for site E at the same time as (c) is presented in (d). The ambient temperature and dewpoint temperature are represented by the black and green lines, respectively. The half barbs, full barbs, and pennants represent 2, 4, and 20 m s^{-1}, respectively. The red triangle represents the level of the PBL top calculated using the bulk *Ri* method with a critical value of 0.25. Vertical profiles of (e) bulk *Ri*, (f) virtual potential temperature (θ_v), (g) relative humidity (RH), (h) wind speed, and (i) wind direction based on the radiosonde observations at site A at 0600 UTC 11 July 2022. The red dashed line indicates the analyzed PBLH marked by the dashed arrow in (b).

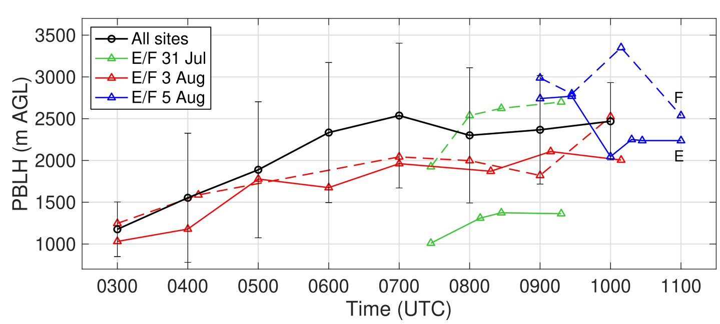

Fig. 3. Diurnal variations of the mean PBLH estimated from 386 IOP radiosonde soundings at six sites (black line). Circles and whiskers denote the mean and standard deviation, respectively. The green, red, and gray lines show the diurnal evolution of PBLH at site E (solid) and site F (dashed) on 31 July, 3 August, and 5 August, respectively.

3.2. A high-ranging PBL case on 28 July

In this section, a deep PBL case on 28 July (Fig. 1(c)) is presented to investigate the sounding-based PBLH difference due to oasis–desert contrast and the associated synoptic conditions. Fig. 4 illustrates the PBL structures during the precipitation-free afternoon on that day (Skew *T*–log *p* diagrams are provided in Fig. S1). At the desert site C, the PBLH reaches 4209 m AGL at 0500 UTC and peaks at 4700 m AGL by 0730 UTC. The combination of this high PBLH and the terrain height of approximately 1500 m results in an exceptionally high PBL top, reaching an elevation of 6200 m above mean sea level (MSL) in the free atmosphere. High PBLHs ranging from 4000 to 6000 m AGL have been reported over desert and arid regions worldwide, such as the Sahara Desert, the Gobi Desert in northern China, New Delhi, and the Tibetan

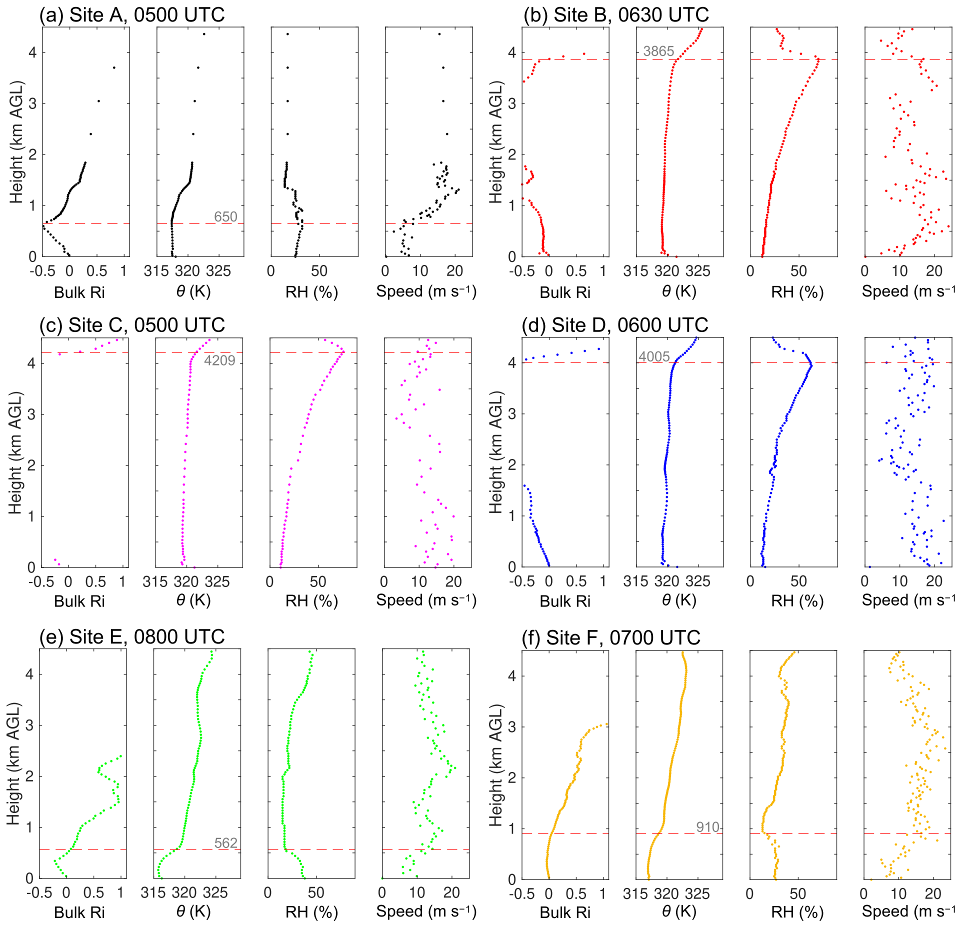

Fig. 4. Vertical profiles of the bulk *Ri*, potential temperature (θ), relative humidity (RH), and wind speed for the radiosonde observations at the six sites on 28 July 2022. The red dashed line indicates the analyzed PBLH. The colors correspond to the radiosonde site colors shown in Fig. 1(b).

Plateau (Chen and Ma, 2025; Chen et al., 2013, 2016). These deep PBLs are expected to facilitate the exchange of heat and momentum between the surface and the upper part of the troposphere.

In contrast, the oasis sites A and E exhibit significantly lower PBLHs. During 0400–0500 UTC, the PBLHs at site A were ~700 m AGL (Fig. 4(a)). At site E, which features lower surface temperature (c.f., Fig. 4(c) and Fig. 4(e)), the PBLHs increase from 416 m AGL to only 562 m AGL from 0700 to 0800 UTC. Located close to the oasis area, the desert site F shows slightly higher PBLH (910 m AGL) than the oasis site E but is significantly lower in height than that of other desert sites (Fig. 4(f)). The evidently lower near-surface air temperature at site F compared to other desert sites suggests that the cooler air masses from irrigated areas have influenced the desert site F. Although the WRF simulation reproduces PBLHs exceeding 4000 m AGL over the desert region, it fails to capture the relatively low PBL at site F. This bias is likely related to the overestimated low-level southerlies, which inhibit the southward transport of cooler air masses from the irrigated area (Fig. S2).

Synoptic analysis indicates that the IOP region was influenced by a large-scale upper-level cold low (Fig. S3(a)). When the cold low approached the region, the advection of colder air aloft increased the environmental lapse rate by cooling the mid–upper troposphere more strongly than the near-surface layer (Fig. S3(b)), and the reduced static stability was expected (see the higher boundary of low Brunt–Väisälä frequency on 28 July in Fig. S3(c)). On the other hand, situated between an upstream shortwave trough base and a downstream ridge, the region was characterized by positive vorticity advection, creating enhanced large-scale mean ascent on that day. This synoptic pattern allowed the boundary layer to grow more easily during daytime heating.

At around 0700 UTC, a distinct radar fine line along the oasis–desert border (between sites E and F) was detected, indicating the presence of a convergent boundary associated with thermal circulations. Approximately 1 h later, discrete convective storms were observed initiating along this convergent boundary (Meng et al., 2024; their Fig. 8e), eventually developing into an organized mesoscale convective system.

4. Conclusions

This study examined the PBLH characteristics over a sharp vegetation-contrast area in North China, utilizing hundreds of radiosonde observations from the DECODE field campaign in the summer of 2022. The fine temporal and spatial resolution sounding data reveal the PBLH seldom observed in this oasis–desert region during the daytime, particularly in the afternoon when conventional operational radiosonde data are unavailable. Throughout the entire IOP periods from 8 July to 5 August 2022, sounding data at 1-s intervals were collected from 695 valid radiosondes. A total of 386 soundings featuring a well-mixed boundary layer during the day were selected to manually estimate the PBLHs at six sites situated across different land uses, including irrigated croplands and deserts.

From 1000 to 1800 LST, the average PBLH across the six IOP sites was approximately 2000 m AGL, with a diurnal peak of around 2500 m AGL. In the presence of large-scale mean ascent, this region occasionally experiences a super high PBL, reaching elevations of approximately 6000 m MSL in the free atmosphere. Due to the thermal contrast between oasis and desert, the oasis sites generally exhibit lower PBLHs than the desert sites; however, the difference carries significant uncertainty, ranging from approximately 200 m to over 1000 m.

Severe storms that initiate locally in this irrigated region not only impact the nearly 600 000 residents here, but also affect downstream areas in eastern China through upscale storm growth and propagation (Huang et al., 2019). Accurately depicting the PBLH in this region is essential for modeling regional convective processes and ecosystems. Further research is needed to enhance the capability of numerical simulations in capturing the PBLH in this oasis–desert area for both weather and climate modeling.

Fundings

This study was supported by the National Natural Science Foundation of China [grant numbers 42030604, 42530601, and 42275006].

Acknowledgments

The authors thank all the participants who assisted in collecting the radiosonde observations. The DECODE radiosonde data are available from the corresponding author upon request for research purposes.

Supplementary materials

Supplementary material associated with this article can be found, in the online version, at doi:10.1016/j.aosl.2026.100782.

References

Beyrich, F., 1997. Mixing height estimation from sodar data – a critical discussion. Atmos. Environ. 31 (23), 3941–3953. doi:10.1016/S1352-2310(97)00231-8.

Chan, K.M., Wood, R., 2013. The seasonal cycle of planetary boundary layer depth determined using COSMIC radio occultation data. J. Geophys. Res. Atmos. 118 (22), 12422–12434. doi:10.1002/2013JD020147.

Chen, X., Škerlak, B., Rotach, M.W., Añel, J.A., Su, Z., Ma, Y., Li, M., 2016. Reasons for the extremely high-ranging planetary boundary layer over the western Tibetan Plateau in winter. J. Atmos. Sci. 73 (5), 2021–2038. doi:10.1175/JAS-D-15-0148.1.

Chen, X., Añel, J.A., Su, Z., de la Torre, L., Kelder, H., van Peet, J., Ma, Y., 2013. The deep atmospheric boundary layer and its significance to the stratosphere and troposphere exchange over the Tibetan Plateau. PLoS One 8 (2), e56909. doi:10.1371/journal.pone.0056909.

Chen, X., Ma, Y., 2025. The unique atmospheric boundary layer over the Tibetan Plateau. Chin. Sci. Bull. 70 (24), 4180–4187. doi:10.1360/TB-2024-1294. (in Chinese)

Dai, C., Wang, Q., Kalogiros, J.A., Lenschow, D.H., Gao, Z., Zhou, M., 2014. Determining boundary-layer height from aircraft measurements. Bound.-Lay. Meteorol. 152 (3), 277–302. doi:10.1007/s10546-014-9929-z.

Eresmaa, N., Karppinen, A., Joffre, S.M., Räsänen, J., Talvitie, H., 2006. Mixing height determination by ceilometer. Atmos. Chem. Phys. 6 (6), 1485–1493. doi:10.5194/acp-6-1485-2006.

Garratt, J., 1994. Review: the atmospheric boundary layer. Earth-Sci. Rev. 37 (1–2), 89–134. doi:10.1016/0012-8252(94)90026-4.

Guo, J., Miao, Y., Zhang, Y., Liu, H., Li, Z., Zhang, W., He, J., Lou, M., Yan, Y., Bian, L., Zhai, P., 2016. The climatology of planetary boundary layer height in China derived from radiosonde and reanalysis data. Atmos. Chem. Phys. 16 (20), 13309–13319. doi:10.5194/acp-16-13309-2016.

Han, Y., Wang, C., Yan, J., Li, X., 2017. Development and application of new boundary layer meteorological sounding system. Meteorol. Sci. Tech. 45 (5), 804–810. doi:10.19517/j.1671-6345.20160615. (in Chinese)

Hennemuth, B., Lammert, A., 2006. Determination of the atmospheric boundary layer height from radiosonde and lidar backscatter. Bound.-Lay. Meteorol. 120 (1), 181–200. doi:10.1007/s10546-005-9035-3.

Hu, X.M., Nielsen-Gammon, J.W., Zhang, F., 2010. Evaluation of three planetary boundary layer schemes in the WRF model. J. Appl. Meteorol. Clim. 49 (9), 1831–1844. doi:10.1175/2010JAMC2432.1.

Huang, Y., Meng, Z., Li, W., Bai, L., Meng, X., 2019. General features of radar-observed boundary layer convergence lines and their associated convection over a sharp vegetation-contrast area. Geophys. Res. Lett. 46 (5), 2865–2873. doi:10.1029/2018GL081714.

Kalmus, P., Ao, C.O., Wang, K.-N., Manzi, M.P., Teixeira, J., 2022. A high-resolution planetary boundary layer height seasonal climatology from GNSS radio occultations. Remote Sens. Environ. 276, 113037. doi:10.1016/j.rse.2022.113037.

Kawase, H., Yoshikane, T., Hara, M., Kimura, F., Sato, T., Ohsawa, S., 2008. Impact of extensive irrigation on the formation of cumulus clouds. Geophys. Res. Lett. 35 (1), L01806. doi:10.1029/2007GL032435.

Liu, H., Meng, Z., Zhu, Y., Huang, Y., 2023. Convection initiation associated with a boundary layer vonvergence line over a real-world sharp vegetation-contrast area. Mon. Wea. Rev. 151 (5), 1189–1212. doi:10.1175/MWR-D-22-0083.1.

Meng, Z., Meng, X., Wang, C., Huang, Y., Zhang, S., Liu, H., Zhang, M., et al., 2024. Desert-oasis convergence line and deep convection experiment (DECODE). Bull. Am. Meteorol. Soc. 105 (12), E2355–E2384. doi:10.1175/BAMS-D-23-0222.1.

Sato, T., Kimura, F., Hasegawa, A.S., 2007. Vegetation and topographic control of cloud activity over arid/semiarid Asia. J. Geophys. Res. 112 (D24), D24109. doi:10.1029/2006JD008129.

Sawyer, V., Li, Z., 2013. Detection, variations and intercomparison of the planetary boundary layer depth from radiosonde, lidar and infrared spectrometer. Atmos. Environ. 79, 518–528. doi:10.1016/j.atmosenv.2013.07.019.

Seibert, P., Beyrich, F., Gryning, S.-E., Joffre, S., Rasmussen, A., Tercier, P., 2000. Review and intercomparison of operational methods for the determination of the mixing height. Atmos. Environ. 34, 1001–1027. doi:10.1016/S1352-2310(99)00349-0.

Seidel, D.J., Ao, C.O., Li, K., 2010. Estimating climatological planetary boundary layer heights from radiosonde observations: Comparison of methods and uncertainty analysis. J. Geophys. Res. Atmos. 115 (D16), D16113. doi:10.1029/2009JD013680.

Seidel, D.J., Zhang, Y., Beljaars, A., Golaz, J.-C., Jacobson, A.R., Medeiros, B., 2012. Climatology of the planetary boundary layer over the continental United States and Europe. J. Geophys. Res. Atmos. 117 (D17), D17106. doi:10.1029/2012JD018143.

Stull, R.B., 1988. An introduction to boundary layer meteorology. Springer, Netherlands, Dordrecht, p. 670. doi:10.1007/978-94-009-3027-8.

Vogelezang, D.H.P., Holtslag, A.A.M., 1996. Evaluation and model impacts of alternative boundary-layer height formulations. Bound.-Lay. Meteorol. 81 (3), 245–269. doi:10.1007/BF02430331.

Xiu, A., Pleim, J. E., 2001. Development of a land surface model. Part I: Application in a mesoscale meteorological model. J. Appl. Meteorol., 40(2), 192–209. doi:10.1175/1520-0450(2001)040<0192:DOALSM>2.0.CO;2.

Zhou, L., 2021. Diurnal asymmetry of desert amplification and its possible connections to planetary boundary layer height: a case study for the Arabian Peninsula. Clim. Dyn. 56 (9), 3131–3156. doi:10.1007/s00382-021-05634-x.